Journal of Power Sources 195 (2010) 4370–4374

Contents lists available at ScienceDirect

Journal of Power Sources

journal homepage: www.elsevier.com/locate/jpowsour

Short communication

Synthesis of fcc Mg–Ti–H alloys by high energy ball milling: Structure and electrochemical hydrogen storage properties

Steeve Rousselot, Daniel Guay, Lionel Roué*

INRS - Énergie, Matériaux et Télécommunications, 1650 Blvd. Lionel-Boulet, Varennes, Québec, Canada J3X 1S2

ARTICLE INFO

Article history:
Received 15 December 2009
Received in revised form
22 December 2009
Accepted 22 December 2009
Available online 21 January 2010

Keywords:
Mechanical alloying
Metal hydride
Mg–Ti based alloys
Ni-MH batteries
Rietveld refinement

ABSTRACT

Mg–Ti–H alloys were synthesized by high energy ball milling from equimolar mixtures of $MgH_2 + TiH_2$, MgH_2 + Ti and Mg + TiH_2 in the presence of 10 wt.% Pd. X-ray diffraction analyses combined with Rietveld refinement revealed that after 60 h of milling, all as-milled Mg–Ti–H alloys are made of two face-centered-cubic (fcc) phases, with lattice parameters ~4.47 and ~4.25 Å, in different proportions depending on the composition of the initial mixture. The Mg–Ti–H alloys displayed a similar electrochemical behavior, *i.e.* their hydrogen discharge capacity was highest during the first cycle and then decreased rapidly with cycling. The maximum discharge capacities of the 60 h-milled $MgH_2 + TiH_2$, MgH_2 + Ti and Mg + TiH_2 materials were 300, 443 and 454 mAh g^{-1}, respectively. No apparent correlation could be established between the maximum discharge capacity of the Mg–Ti–H materials and the two fcc phase proportion.

1. Introduction

Mg–Ti-based hydrides are promising materials for various applications such as negative electrodes for Ni-MH batteries [1–10], H_2 sources for fuel cells [11,12], switchable mirrors for smart solar collectors [13–16] and optical hydrogen detectors [18]. Their face-centered-cubic (fcc) structure in hydrogenated state is most likely responsible for their excellent hydriding kinetic properties [19,20].

The synthesis of Mg–Ti alloys requires non-standard alloying methods since, as illustrated by the Mg–Ti phase diagram [21], this system is almost immiscible in equilibrium conditions. Metastable single-phase Mg–Ti thin films have been successfully synthesized over a large composition range by means of electron-beam and magnetron co-sputter deposition techniques [1–4,13–20]. However, these synthesis methods are not suitable for large-scale and low-cost production of bulk Mg–Ti materials as required for Ni-MH battery and fuel cell applications. In this regard, mechanical alloying has demonstrated its high efficiency for producing metastable Mg–Ti alloys starting from elemental Mg and Ti powders [5–11,22–28]. The crystal structure of the end-product appears to be very sensitive to the milling conditions. Indeed, depending on the starting powder composition, milling duration, ball-to-powder mass ratio, nature of process control agents and milling tools, the milled Mg–Ti products exhibit a hexagonal-close-packed (hcp) structure, a body-centered-cubic (bcc) structure, a face-centered-cubic (fcc) structure or a mixture of these. The strong influence of the milling conditions on the structure of milled Mg–Ti materials suggests a close relationship to the plastic deformation process that occurs during ball milling, which in turn is related to the impact energy imparted to the material by the milling balls [28].

Direct synthesis of Mg–Ti–H hydrides by ball milling of MgH_2 with Ti or TiH_2 was also performed [12,29–32]. With the addition of a small amount of Ti (8 and 13 mol.%), milling of MgH_2 leads to the formation TiH_2 together with Mg, γ-MgH_2 and trace amounts of the starting MgH_2 powder, *i.e.* no Mg–Ti–H hydride is formed [29,30]. With a higher Ti content (20 and 50 mol.%), Asano and Akiba [12] reported the formation of Mg–Ti–H fcc phases with a lattice parameter of 4.45 Å. Choi et al. focused on the milling of MgH_2 with various TiH_2 amounts (9–25 mol.%) under high H_2 pressure, but no Mg–Ti–H hydride phase was found in the as-milled products [31,32].

In a previous paper [9], we have examined in detail the structure and electrochemical hydriding behavior of $Mg_{100-x}Ti_x$ materials (with x ranging from 20 to 80) prepared by ball milling from elemental Mg and Ti powders in the presence of 10 wt.% Pd. It was found that the $Mg_{50}Ti_{50}$ alloy possessed the highest hydrogen discharge capacity of all Mg–Ti alloys (*i.e.* 475 mAh g^{-1}) and that the bcc/hcp phase mixture initially present in the as-milled material was transformed into a fcc phase with a lattice parameter of 4.46 Å upon electrochemical hydrogenation.

In the present study, fcc Mg–Ti–H based alloys are directly synthesized by high energy ball milling from the mixtures of

* Corresponding author. Tel.: +1 450 929 8185; fax: +1 450 929 8102.
E-mail address: roue@emt.inrs.ca (L. Roué).

0378-7753/$ – see front matter © 2010 Elsevier B.V. All rights reserved.
doi:10.1016/j.jpowsour.2009.12.138

$MgH_2 + TiH_2$, MgH_2 + Ti and Mg + TiH_2 (with a molar ratio of 1:1) in the presence of 10 wt.% Pd. The structure and electrochemical hydrogen storage properties of these different materials are reported and compared to those previously obtained with $Mg_{50}Ti_{50}$–10 wt.% Pd alloy prepared from elemental Mg and Ti powders [9].

2. Experimental

Pure Mg (99.9%, chips, Norsk Hydro), MgH_2 (98%, -325 mesh, ABCR GmbH & Co. KG), Ti (99.5%, -325 mesh, Alfa Aesar) and TiH_2 powders (99%, -325 mesh, Alfa Aesar) were used as starting materials. Three series of mixtures were prepared, namely $MgH_2 + TiH_2$, MgH_2 + Ti and Mg + TiH_2 (all with a molar ratio of 1:1). 10 wt.% of Pd powder (99.9%, -325 mesh, Alfa Aesar) was added as a hydrogenation catalyst [10]. Ball milling was conducted in cylindrical stainless steel crucibles (55 ml) with three stainless steel balls (one 14 mm and two 11 mm diameter). The ball-to-powder mass ratio was 9:1 for all experiments. The container was sealed under argon atmosphere and placed in a vibratory type mill (Spex 8000M). Milling of the powders was performed for various periods of time (1–60 h). The milling yield, defined as the mass ratio of the powder after and before milling, was never less than 70% for all experiments, suggesting the absence of excessive cold welding of the powders on the milling tools during the milling process.

After ball milling, energy dispersive X-ray (EDX) analysis of the samples revealed that the Mg:Ti atomic ratio in the different samples was close to 40:60 (compared to a nominal Mg:Ti atomic ratio of 50:50) suggesting the predominant sticking of Mg on the milling tools. In all cases, the EDX analysis showed that the iron content was less than 1 at.%, reflecting the limited erosion of the container and balls, even after 60 h of milling. Hydrogen content of the as-milled materials was determined by a LECO TCH600 hydrogen determinator.

The specific surface area of the powders was measured by Kr adsorption (multipoint BET) using a Quantachrome Autosorb Automated Gas Sorption system.

The materials were characterized by X-ray diffraction (XRD) using a Bruker D8 diffractometer with Cu Kα radiation. Structure refinement was performed according to the Rietveld method [33] using GSAS and EXPGUI softwares [34,35].

Electrochemical charge/discharge cycling tests were carried out on an Arbin BT2000 battery tester at room temperature in a 6 M KOH electrolyte using a three-electrode cell. The working electrode was made of a mixture of 100 mg of active material, 800 mg of graphite and 20 mg of carbon black. The counter electrode was a nickel wire and the reference electrode was an Hg/HgO electrode. The working electrode was charged at a current density of $-200\ mA\ g^{-1}$ for 3 h and discharged at $20\ mA\ g^{-1}$ followed by a deeper discharge at $5\ mA\ g^{-1}$ with a cut off potential fixed at −0.4 V vs. Hg/HgO. The masses of Mg, Ti and Pd were considered for the calculation of the hydrogen capacity expressed in $mAh\ g^{-1}$ of active material.

3. Results and discussion

3.1. Structural analysis

3.1.1. $MgH_2 + TiH_2$

Fig. 1 depicts the evolution of the XRD patterns of an equimolar mixture of MgH_2 and TiH_2 as a function of the milling time. For $t = 0$, curve A shows the characteristic diffraction peaks of α-MgH_2 (tetragonal phase with $a = 4.52$ and $c = 3.02$ Å) at $2\theta = 27.9°$, 35.7°, 39.9°, 54.6° and 57.7° and those of TiH_2 (fcc phase with $a = 4.448$ Å) at $2\theta = 34.9°$, 40.5°, 58.6°, 70.1° and 73.7°. After 1 h of milling (curve B), the diffraction peaks of α-MgH_2 have almost totally disappeared, while those of the fcc phase are still clearly discernible, although their full-width at half-maximum have increased. After 10 h of milling (curve E), the diffraction peaks of α-MgH_2 are no longer discernible, while those of the fcc phase are displaced toward the lower 2θ angle values. This effect is further emphasized after 20 h of milling (curve F). No further change in the XRD pattern is observed if milling is prolonged up to 60 h (curve G).

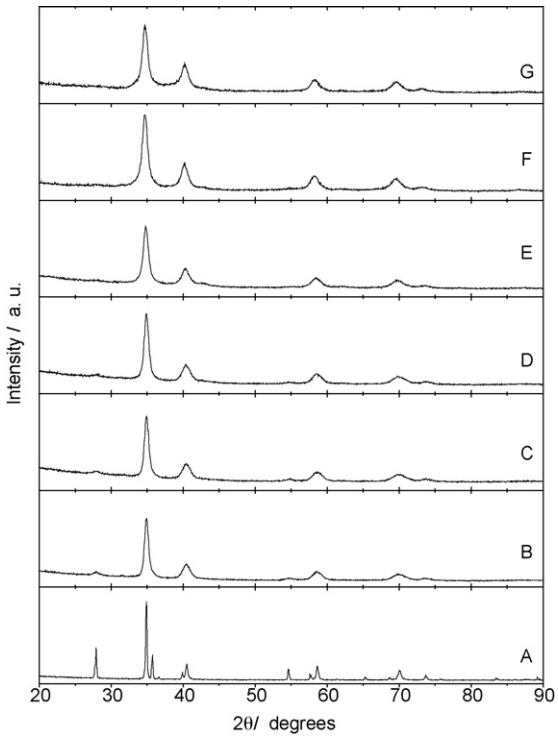

Fig. 1. X-ray diffraction patterns of milled $MgH_2 + TiH_2$. The milling time is (A) 0, (B) 1, (C) 2, (D) 5, (E) 10, (F) 20, and (G) 60 h.

The evolution with milling time of the lattice constant and crystallite size of the fcc phase is depicted in Fig. 2A and B, respectively. The lattice constant of the fcc phase, a_{fcc}, does not change during the first few hours of milling. After 5 h of milling, it increases from its initial value of 4.45 Å to its final value of 4.48 Å. This change of the lattice constant occurs over a period of ∼10 h of milling. In contrast, the variation of the crystallite size occurs markedly faster at the beginning of the milling period, changing from ∼52 to ∼12 nm during the first hour of milling. Beyond the first hour of milling there is no significant change of the crystallite size as it evolves from ∼12 to ∼5 nm when milling is prolonged up to 60 h.

The XRD pattern of $MgH_2 + TiH_2$ milled 60 h (Fig. 1, curve G) is distinctly different from that of milled Mg + Ti. In the latter case, we showed that the milled powder was made of a mixture of bcc (∼84 wt.%) and hcp (∼16 wt.%) and no fcc phase could be identified in the as-milled material [9]. However, electrochemical hydrogenation of milled Mg + Ti led to the formation of a fcc phase, whose lattice parameter was $a = 4.46$ Å [9], close to that found in this study by milling an equimolar mixture of MgH_2 and TiH_2 ($a = 4.48$ Å). As seen elsewhere [7,8], this transformation from a mixture of bcc and hcp to fcc upon hydrogenation is irreversible and de-hydrogenation leads only to a shift of the main (1 1 1) diffraction peak of the fcc phase toward the larger 2θ angle values (from $2\theta = 34.7°$ to $2\theta = 35.0°$), indicating a slight decrease of the lattice parameter due to a change (decrease) of the H content. Thus, the formation of a Mg–Ti–H fcc phase upon milling of $MgH_2 + TiH_2$ is consistent with what is known about the hydrogenation characteristics of milled Mg + Ti.

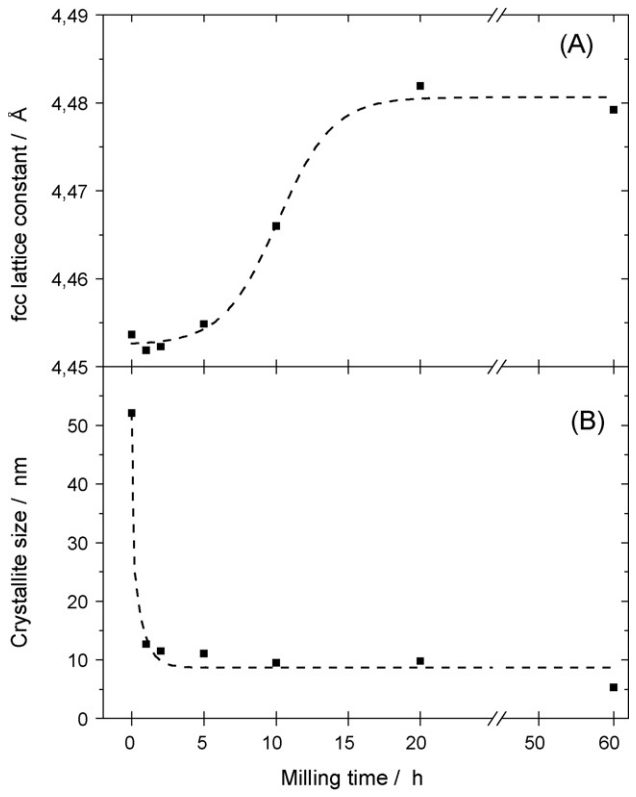

Fig. 2. Variation of (A) the lattice constant of the fcc phase and (B) the crystallite size of $MgH_2 + TiH_2$ with respect to the milling time.

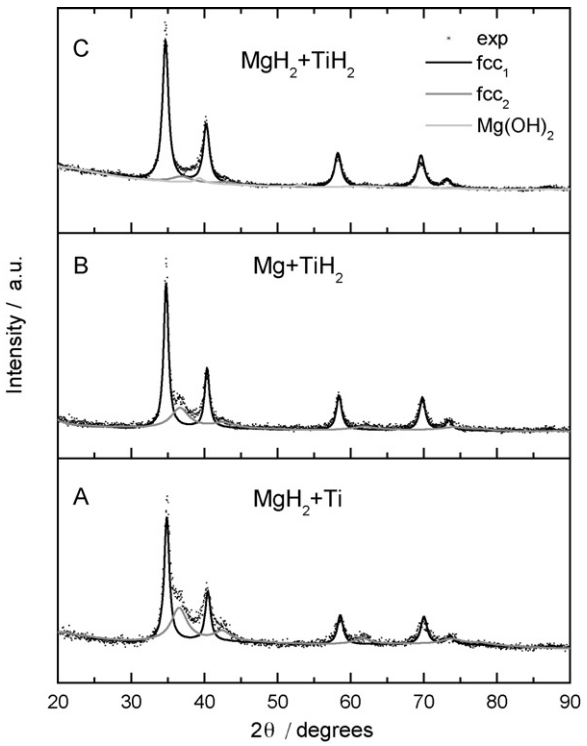

Fig. 3. X-ray diffraction patterns of (A) $MgH_2 + Ti$, (B) $Mg + TiH_2$ and (C) $MgH_2 + TiH_2$ milled for 60 h. The contribution of the various phases to the experimental XRD pattern is also shown.

We have shown elsewhere that milling of pure α-MgH_2 leads to the formation of γ-MgH_2 and that, after 10 h of milling, the weight ratio between α- and γ-MgH_2 is ~3 [36]. A similar conclusion was reached elsewhere [29]. In the present case, the milling of α-MgH_2 in the presence of TiH_2 suppresses this phase transformation and the characteristic diffraction peaks of γ-MgH_2 are not observed in the XRD patterns of Fig. 1.

It is interesting to note that a_{fcc} stays constant during the first 5 h of milling and only starts to increase when the diffraction peaks of α-MgH_2 are no longer discernible. Since no new diffraction peaks are discernible in the XRD patterns, the disappearance of the diffraction peaks of α-MgH_2 must be related to a pronounced reduction of the crystallite size of that phase. It is hypothesized that dissolution of MgH_2 into TiH_2 occurs only once the crystallites of α-MgH_2 are small enough, thereby causing an increase of the lattice parameter of the fcc phase. Such a behavior may result from the brittle nature of the MgH_2 and TiH_2 materials inducing the formation of granular particles during the first stage of milling rather than lamellar particles for ductile materials [37]. Consequently, the diffusion paths are longer for brittle materials and a critical grain size must be reached for inducing the alloying reaction.

3.1.2. *Comparison between Mg + TiH_2, MgH_2 + Ti and MgH_2 + TiH_2*

Equimolar mixtures of $MgH_2 + Ti$ and $Mg + TiH_2$ were milled for 60 h (*i.e.* long enough to obtain a steady state structure) and the XRD patterns of the resulting materials are shown in Fig. 3A and B, respectively. The XRD pattern of $MgH_2 + TiH_2$ milled for 60 h is also shown for comparison (Fig. 3C). The nominal Mg:Ti atomic ratio of these mixtures is the same (1:1) but they differ by the source of the hydrogen atoms (either MgH_2 or TiH_2) and the H/(Mg + Ti) atomic ratio, which is either 1 or 2.

As seen on the XRD patterns of milled $MgH_2 + Ti$ (Fig. 3A) and milled $Mg + TiH_2$ (Fig. 3B), five intense peaks located at $2\theta = 34.9°$, 40.5°, 58.6°, 70.1° and 73.7° are clearly discernable. These peaks correspond to the (1 1 1), (2 0 0), (2 2 0), (3 1 1) and (2 2 2) reflections of an fcc phase, respectively. Indeed, these peaks are at the same position as those found previously in $MgH_2 + TiH_2$ milled for 60 h (Fig. 3C). In addition, a shoulder is clearly discernible on the high 2θ angle side of the (1 1 1) and (2 0 0) diffraction peaks suggesting a second phase is present in these compounds. These XRD patterns do not exhibit any sign of un-reacted Mg, MgH_2, Ti and TiH_2.

A Rietveld refinement analysis was performed on the XRD patterns of Fig. 3 to determine the phase composition of the compounds. As seen in Table 1, the XRD patterns of all compounds ($MgH_2 + Ti$, $Mg + TiH_2$ and $MgH_2 + TiH_2$) could be accounted for on

Table 1
Results of Rietveld refinement analysis of mechanically milled Mg–Ti–H materials.

Compounds	fcc1			fcc2			$Mg(OH)_2$			
	Lattice constant (Å)	Crystallite size (nm)	Abundance (wt.%)	Lattice constant (Å)	Crystallite size (nm)	Abundance (wt.%)	Lattice constant		Crystallite size (nm)	Abundance wt.%
							a (Å)	*c* (Å)		
$MgH_2 + Ti$	4.46	10	60	4.26	3	40	–	–	–	–
$Mg + TiH_2$	4.47	11	73	4.25	3	27	–	–	–	–
$MgH_2 + TiH_2$	4.48	9	83	4.22	3	10	3.06	4.55	7	7

the basis of two different fcc phases, fcc_1 and fcc_2, with $a_1 \sim 4.47$ and $a_2 \sim 4.25$ Å. From these data alone, it was not possible to determine the composition of these two phases. However, based on our previous work [9], it can be assumed that the composition of the fcc phase with $a_1 \sim 4.47$ Å is close to 50:50 (Mg:Ti). This would mean that the composition of the fcc phase with $a_2 \sim 4.25$ Å is also close to 50:50. So, assuming that both fcc phases have the same composition, their relative proportion can be obtained from the Rietveld analysis. It is postulated that the difference observed between the *a* lattice parameter of both fcc phases could be due to the presence of hydrogen in one of them (fcc_1). As seen in Table 1, fcc_1 with $a_1 \sim 4.47$ Å accounts for as high as 83 wt.% of as-milled $MgH_2 + TiH_2$ and not more than 60 wt.% in the case of as-milled $MgH_2 + Ti$.

In comparison, it was recently shown that milling of an equimolar mixture of MgH_2 and Ti led to the formation of fcc $Mg_{40}Ti_{60}H_{113}$ (89 wt.%) and hexagonal Mg (11 wt.%) [12]. The lattice parameter of the fcc phase was 4.45 Å, close to the value found in the present study for milled $MgH_2 + TiH_2$, $Mg + TiH_2$ and $MgH_2 + Ti$ (see Table 1).

The appearance of a fcc phase with a ~4.25 Å upon milling a mixture of Mg and Ti has also been reported in the past. For example, Asano et al. noted the formation of a pure fcc phase with lattice parameter 4.31 Å when synthesizing $Mg_{50}Ti_{50}$ alloy using zirconia balls and container in a Fritsch ball mill [28]. Also, Kalisvaart et al. have observed the formation of two fcc phases with lattice parameters 4.25 and 4.44 Å when Mg and Ti powders were milled with stearic acid [5].

The hydrogen content (measured by LECO H determinator) of as-milled $MgH_2 + Ti$ and $Mg + TiH_2$ was 2.02 and 2.23 wt.%, respectively, slightly lower than the nominal H content (2.46 wt.% H including Pd mass). The hydrogen content in as-milled $MgH_2 + TiH_2$ was 1.81 wt.% H. This value corresponds to only ~38% of the nominal H content in the powder (4.78 wt.% H including Pd mass), pointing to dehydrogenation during milling. Indeed, we have observed a slight overpressure in the vial at the end of the milling operation, indicating that hydrogen is released from the compound during the milling process. Moreover, this compound being very reactive, its partial decomposition may occur after opening of the vial in air, as evidenced by the presence of $Mg(OH)_2$ peaks on the XRD pattern (see Fig. 3C and Table 1).

3.2. Electrochemical behavior

The evolution with cycling of the discharge capacities of 60 h-milled $MgH_2 + TiH_2$, $MgH_2 + Ti$ and $Mg + TiH_2$ materials are shown in Fig. 4. The cycling discharge capacities of 20 h-milled Mg + Ti [9] is also shown for comparison. The Mg–Ti–H materials exhibit a similar behavior, *i.e.* their discharge capacity is highest during the first cycle and then decreases continuously with cycling. In contrast, the Mg + Ti sample needs 3 activation cycles before reaching its maximum discharge capacity. It was suggested in a previous study that the activation period observed upon charge/discharge cycling on Mg–Ti alloys may be related to a structural transition from a bcc/hcp phase mixture to a fcc phase that occurs during the first few cycles [9]. The absence of such an activation period on Mg–Ti–H electrodes (Fig. 4) is consistent with this assumption since these materials have a fcc phase structure in their as-prepared state (see Table 1) and thus, no phase transition is expected upon cycling.

The maximum discharge capacities of $MgH_2 + TiH_2$, $MgH_2 + Ti$ and $Mg + TiH_2$ electrodes are 300, 443 and 454 mAh g^{-1} respectively compared to 475 mAh g^{-1} for the Mg + Ti electrode (Fig. 4). Thus, no improvement in terms of electrochemical H-storage capacities is obtained by using Mg–Ti–H compared to Mg–Ti as active material. In addition, as seen in Fig. 4, the capacity decay with cycling is more pronounced on Mg–Ti–H electrodes than on the Mg–Ti electrode. This may be attributed to the higher specific surface area (*i.e.* lower particle size) of the as-milled Mg–Ti–H

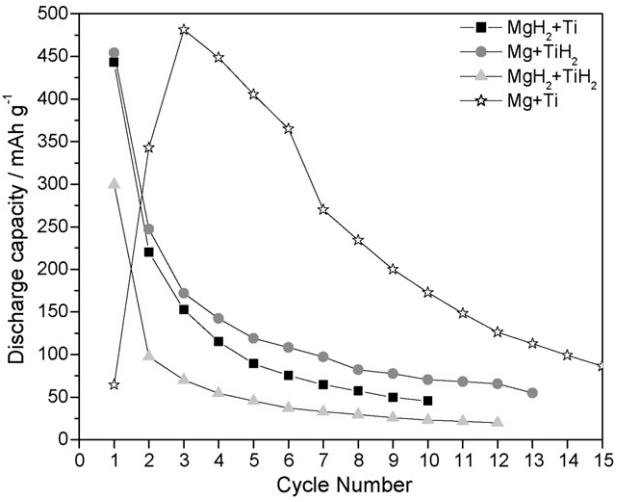

Fig. 4. Evolution with cycling of the discharge capacities of the Mg + Ti, $MgH_2 + TiH_2$, $MgH_2 + Ti$ and $Mg + TiH_2$ electrodes.

materials, accentuating their oxidation rate by the KOH electrolyte and cracking upon cycling as observed with MgNi electrodes made of different particle sizes [38]. The higher specific surface area of as-milled Mg–Ti–H materials is confirmed by BET measurements indicating a specific surface area of 4.95, 1.58 and 0.89 $m^2\ g^{-1}$ for milled $MgH_2 + TiH_2$, $MgH_2 + Ti$ and $Mg + TiH_2$ powders, respectively, compared to only 0.19 $m^2\ g^{-1}$ for milled Mg + Ti powder. This difference can be explained by the brittle characteristic of MgH_2 and TiH_2 powders favouring their fracturing during the milling process whereas cold welding is likely predominant with more ductile Mg and Ti materials. This is in accordance with the comparative morphological observations made between milled MgH_2 and Mg [36].

Kalisvaart et al. have observed the formation of two fcc phases with lattice parameters 4.25 and 4.44 Å for mechanically alloyed Mg–Ti based materials and they concluded that only the phase with the largest lattice constant is electrochemically active for the reversible H-absorption reaction [5]. In the present study, the maximum discharge capacity of the $MgH_2 + TiH_2$ electrode is 300 mAh g^{-1} and *ca.* 450 mAh g^{-1} for $Mg + TiH_2$ and $MgH_2 + Ti$ electrodes (Fig. 4) whereas the abundance of the phase with the larger lattice parameter in these materials is 83, 73 and 60 wt.%, respectively (see fcc1 abundance in Table 1). Thus, no correlation can be established between the maximum discharge capacity of the Mg–Ti–H materials and the abundance of the fcc_1 phase, in contrast to that observed by Kalisvaart et al. [5]. This discrepancy may be related to the irreversible oxidation by contact with air and/or KOH electrolyte in the Mg–Ti–H compounds (especially $MgH_2 + TiH_2$ as discussed before), thus affecting their electrochemical H-storage capacity.

The maximal H-content extracted electrochemically from Mg–Ti–H materials (calculated from their maximal discharge capacity) is 1.12, 1.65 and 1.69 wt.% for $MgH_2 + TiH_2$, $MgH_2 + Ti$ and $Mg + TiH_2$, respectively. These H-content values are lower than those measured in the as-milled powders, which are 1.81, 2.02 and 2.23 wt.%, respectively, as indicated previously. This difference may result from the irreversible oxidation (*i.e.* $Mg(OH)_2$ formation) of the Mg–Ti–H materials by contact with the KOH electrolyte. However, it may also indicate that some H atoms absorbed onto the Mg–Ti–H alloys during their synthesis cannot be desorbed electrochemically. This is consistent with recent theoretical calculations showing that the bonding between Mg and H is weakened by the dissolution of Ti atoms in magnesium hydride, while a stronger interaction exists between Ti and H atoms [39]. As suggested in that

paper, the reduced interaction between Mg and H atoms resulted in favorable breaking of the Mg–H bonds and hence of desorption of hydrogen. However, only a fraction of the hydrogen atoms can be released by the addition of Ti due to the relatively stronger bond between Ti and H atoms. The existence of this stronger bond between Ti and H may explain the partial irreversible hydrogen absorption properties of the Mg–Ti–H materials.

4. Conclusion

It was shown that fcc Mg–Ti–H alloys can be prepared by high energy ball milling of $MgH_2 + TiH_2$, $MgH_2 + Ti$ or $Mg + TiH_2$. All as-milled powders consisted of two fcc phases with lattice parameters ~4.47 and ~4.25 Å. The relative proportion of these two phases varied with the composition of the initial powder mixture. The milled $MgH_2 + TiH_2$, $MgH_2 + Ti$ and $Mg + TiH_2$ electrodes reached their maximum discharge capacity during the first cycle (300, 443 and 454 mAh g^{-1}, respectively). In comparison, a milled Mg + Ti electrode (made of a hcp/bcc phase mixture) required three activation cycles before reaching its maximum discharge capacity (475 mAh g^{-1}). No apparent relation could be established between the maximum discharge capacity of the Mg–Ti–H materials and the relative proportion of the two fcc phases in their as-milled state. Studies on the structural evolution of the Mg–Ti–H materials with cycling should be conducted to shed light on this issue.

Acknowledgements

This work was financially supported by the Natural Sciences and Engineering Research Council (NSERC) and the "Fonds Québecois de la Recherche sur la Nature et les Technologies" (FQRNT).

References

[1] R.A.H. Niessen, P.H.L. Notten, Electrochem. Solid-State Lett. 8 (2005) A534.
[2] P. Vermeulen, R.A.H. Niessen, P.H.L. Notten, Electrochem. Commun. 8 (2006) 27.
[3] P. Vermeulen, R.A.H. Niessen, D.M. Borsa, B. Dam, R. Grissen, P.H.L. Notten, Electrochem. Solid-State Lett. 9 (2005) A520.
[4] P. Vermeulen, E.F.M.J. van Thiel, P.H.L. Notten, Chem. Eur. J. 13 (2007) 9892.
[5] W.P. Kalisvaart, H.J. Wondergem, F. Bakker, P.H.L. Notten, J. Mater. Res. 22 (2007) 1640.
[6] W.P. Kalisvaart, P.H.L. Notten, J. Mater. Res. 23 (2008) 2179.
[7] S. Rousselot, M.P. Bichat, D. Guay, L. Roué, J. Power Sources 175 (2008) 621.
[8] S. Rousselot, M.P. Bichat, D. Guay, L. Roué, ECS Trans. 16 (2009) 91.
[9] S. Rousselot, M.P. Bichat, D. Guay, L. Roué, J. Electrochem. Soc. 156 (2009) A967.
[10] S. Rousselot, A. Gazeau, D. Guay, L. Roué, Electrochim. Acta. 55 (2010) 611.
[11] K. Asano, H. Enoki, E. Akiba, J. Alloys Compd. 478 (2009) 117.
[12] K. Asano, E. Akiba, J. Alloys Compd. 481 (2009) L8.
[13] D.M. Borsa, A. Baldi, M. Pasturel, H. Schreuders, B. Dam, R. Griessen, P. Vermeulen, P.H.L. Notten, Appl. Phys. Lett. 88 (2006) 241910.
[14] D.M. Borsa, R. Gremaud, A. Baldi, H. Schreuders, J.H. Rector, B. Kooi, P. Vermeulen, P.H.L. Notten, B. Dam, R. Griessen, Phys. Rev. B 75 (2007) 205408.
[15] K. Tajima, Y. Yamada, S. Bao, M. Okada, K. Yoshimura, J. Appl. Phys. 103 (2008) 013512.
[16] S. Bao, K. Tajima, Y. Yamada, M. Okada, K. Yoshimura, Solar Energy Mater. Solar Cells 92 (2008) 224.
[17] A. Baldi, D.M. Borsa, H. Schreuders, J.H. Rector, T. Atmakidis, M. Bakker, H.A. Zondag, W.G.J. van Helden, B. Dam, R. Griessen, Int. J. Hydrogen Energy 33 (2008) 3188.
[18] M. Slaman, B. Dam, H. Schreuders, R. Griessen, Int. J. Hydrogen Energy 33 (2008) 1084.
[19] P. Vermeulen, H.J. Wondergem, P.C.J. Graat, D.M. Borsa, H. Schreuders, B. Dam, R. Griessen, P.H.L. Notten, J. Mater. Chem. 18 (2008) 3680.
[20] P. Vermeulen, P.C.J. Graat, H.J. Wondergem, P.H.L. Notten, Int. J. Hydrogen Energy 33 (2008) 5646.
[21] A.A. Nayeb-Hashemi, J.B. Clark, Phase Diagrams of Binary Magnesium Alloys, ASM International, Metals Park, OH, 1998.
[22] C. Suryanarayana, F.H. Froes, J. Mater. Res. 5 (1990) 1880.
[23] M. Hida, K. Asai, Y. Takemoto, A. Sakakibara, Mater. Trans. 37 (1996) 1679.
[24] F. Sun, F.H. Froes, J. Alloys Compd. 340 (2002) 220.
[25] G. Liang, R. Schulz, J. Mater. Sci. 38 (2003) 1179.
[26] K. Asano, H. Enoki, E. Akiba, Mater. Trans. 48 (2007) 121.
[27] K. Asano, H. Enoki, E. Akiba, J. Alloys Compd. 486 (2009) 115.
[28] K. Asano, H. Enoki, E. Akiba, J. Alloys Compd. 480 (2009) 558.
[29] G. Liang, J. Huot, S. Boily, A. Van Neste, R. Schulz, J. Alloys Compd. 292 (1999) 247.
[30] C.X. Shang, M. Bououdina, Y. Song, Z.X. Guo, Int. J. Hydrogen Energy 29 (2004) 73.
[31] Y.J. Choi, J. Lu, H.Y. Sohn, Z.Z. Fang, J. Power Sources 180 (2008) 491.
[32] Y.J. Choi, J. Lu, H.Y. Sohn, Z.Z. Fang, E. Rönnebro, J. Phys. Chem. C 113 (2009) 19344.
[33] R.A. Young, The Rietveld Method, Oxford University Press, Oxford, 1993.
[34] A.C. Larson, R.B Von Dreele, GSAS–General Structure Analysis System, Los Alamos National Laboratory Report LAUR 86-748, 2000.
[35] H. Toby, J. Appl. Cryst. 34 (2001) 213.
[36] M.H. Grosjean, M. Zidoune, L. Roué, J.Y. Huot, Int. J. Hydrogen Energy 31 (2006) 109.
[37] C. Suryanarayana, Prog. Mater. Sci. 46 (2001) 1.
[38] C. Rongeat, L. Roué, J. Power Sources 132 (2004) 302.
[39] Y. Song, Z.X. Guo, R. Yang, Mater. Sci. Eng. A 365 (2004) 73.